Nuclear Instruments and Methods in Physics Research A 350 (1994) 368–378
North-Holland

NUCLEAR
INSTRUMENTS
& METHODS
IN PHYSICS
RESEARCH
Section A

The X-ray energy response of silicon Part A. Theory

G.W. Fraser *, A.F. Abbey, A. Holland, K. McCarthy, A. Owens, A. Wells
X-ray Astronomy Group, Department of Physics and Astronomy, University of Leicester, Leicester LE1 7RH, UK

Received 24 May 1994

In this, the first part of a two-part study of the interaction of soft X-rays with silicon, motivated by the calibration requirements of CCD imaging spectrometers in astronomy, we describe a Monte Carlo model of X-ray energy loss whose products are the energy- and temperature-dependences of (i) W, the average energy required to create an electron-hole pair, and (ii) the Fano factor F. W and F have invariably been treated as material constants in previous analyses of Si X-ray detector performance. We show that in fact, at constant detector temperature T, W is an increasing function of X-ray energy for $E < 0.5$ keV while F is predicted to increase slowly with E. The temperature coefficient dW/dT has a calculated value $\sim 1 \times 10^{-4}$ K^{-1} at a typical CCD operating temperature of 170 K. We discuss the practical implications of these results.

Finally, we describe our separate calculations of the near-edge variation of CCD quantum detection efficiency arising from silicon K-shell Extended X-ray Absorption Fine Structure (EXAFS).

1. Introduction

The interaction of soft X-ray photons (energies $0.05 < E < 10$ keV) with silicon is a detector physics topic of fundamental interest in many fields [1–7]. In X-ray astronomy, photon-counting silicon charged coupled devices (CCDs) will be the prime spectroscopic detectors for almost all satellite observatories operational in the next decade. The Leicester X-ray Astronomy group is presently involved in the development of CCD focal plane arrays for two major experiments: the Joint European X-ray Telescope (JET-X) for the Russian Spectrum X-Gamma mission [8] and the European Photon Imaging Camera (EPIC) [9] for ESA's XMM Observatory.

The first modern instrument to combine high throughput X-ray optics with the resolving power of a silicon detector ($E/\Delta E > 50$ for 6 keV X-rays) was the US Broad Band X-ray Telescope (BBXRT), a cooled, segmented Si (Li) detector at the focus of gold-coated conical foil optics, carried into orbit by the Shuttle in December 1990. The BBXRT X-ray spectrum of the Crab Nebula [10] contains spurious emission/absorption line features correlated with the K edge of oxygen of 0.54 keV, with the K edge of silicon at 1.839 keV and, possibly, with the 2.20–3.425 keV M edges of gold. These instrumental artefacts lie in precisely the same energy range as emission and absorption features expected from H- and He-like Si, S and Ar in cosmic plasmas.

From the example of BBXRT and from other evidence, it is clear that physical models of X-ray mirror and solid state detector responses must now be developed to a higher level of precision than hitherto considered acceptable in X-ray astronomy, if the scientific return from future experiments is not to be compromised. In parallel, we believe that "traditional" methods of energy calibration, using only sparse sets of isolated X-ray lines [8,11,12], must be supplemented by measurements at synchrotron sources, continuously tunable in energy in $\sim$ eV steps.

The present paper, which is restricted to the theoretical characterisation of Si detector response, addresses two concerns:

(i) That small ($\sim$ percent) departures from perfect linearity must exist in silicon-based X-ray detectors, in particular discontinuities in the W parameter at the Si L (99 and 148 eV) and K absorption edges. W is, of course, the average energy required to produce an internal electron–hole pair (Section 2 below). Such non-linearities, difficult to detect using traditional methods of energy calibration, are, however, well documented for other classes of (astronomical) X-ray detector. Lamb et al. [13] describe post-flight synchrotron studies of discontinuous changes in "electron gain" E/W for the Spacelab 1 gas scintillation proportional counter (GSPC) in the vicinity of the Xe L edges (4.78–5.45 keV). In flight, these discontinuities gave rise to a spurious narrow line feature at 4.8 keV in the X-ray spectrum of the Crab Nebula. More recently, Jahoda and McCammon [14] have reported discontinuities in the response of an argon–methane proportional counter across

* Corresponding author.

SSDI 0168-9002(94)00661-P

the Ar L_{II}, L_{III} edges at 250 eV, while Tsumemi et al. [15] have described a gain change across the Xe K edge (34.56 keV) in a Xe–CO_2 counter flown on the Japanese Ginga X-ray astronomy satellite. Finally, Zulliger et al. [16] have reported a ~ 1% gain non-linearity over the Ge K edge (11.10 keV) in the response of a Ge(Li) X-ray detector.

(ii) That Extended X-ray Absorption Fine Structure (EXAFS) effects must give rise to oscillatory variations in detector quantum efficiency Q (counts/photon) at energies just above the atomic absorption edges of the detector constituents (Si, O and N – from the nitride passivation layer – in the particular case of CCDs). EXAFS effects in solid state X-ray detector response, arising from the scattering of the outgoing spherical photoelectron wave by nearest neighbour atoms in the lattice [17], have been little investigated to date. The synchrotron measurements of Krumrey et al. [2] on a photon-counting Si(Li) detector indicate Si K-shell EXAFS-related variations in $Q(E)$ at the ~ 3% level. Cho et al. [18] have reported significant EXAFS modulation of the current responses of both a silicon surface barrier detector and a lead silicate glass microchannel plate detector in a ~ 150 eV energy band extending upwards from the Si K edge. We note that such current response measurements [4–6,19] effectively record the ratio Q/W and so confuse the effects of EXAFS with possible variations in W(E) (above).

Section 3 below describes what we believe to be the first ab initio calculation of the energy (and temperature) variation of the W parameter for X-rays in silicon. The energy range (0.05–8 keV) of this linearity study includes both the L- and K-shell absorption edges. Our Monte Carlo analysis, like those of the Universidade de Coimbra group [20,21] for Xe GSPCs and of Akkerman et al. [22] for CsI X-ray photocathodes, utilises microscopic cross-sections for electron interaction to model the creation of a secondary electron population by energy loss from a number of X-ray induced (photo-Auger, Coster–Kronig and shake-off) primaries. In addition to $W(E, T)$, the model produces estimates of the X-ray Fano factor $F(E, T)$. Here, T denotes the detector operating temperature. Assuming a Gaussian pulse height distribution, W and F determine the intrinsic FWHM energy resolution of the detector via the equation:

$$\Delta E = (8 \ln 2)^{0.5} W\{FE/W\}^{0.5}. \quad (1)$$

No measurements of the energy dependence of the Fano factor have previously been reported for silicon. In Xe, however, a sawtooth variation of $F(E)$, following the total photoionisation cross-section for the gas, is now well-documented experimentally and interpreted in terms of mechanisms [20] which are likely to operate in all X-ray detector media.

Section 4 of the paper, addressing the second of our calibration concerns, predicts the near-edge variation in CCD quantum efficiency arising from the known oscillatory variation [17] in the linear absorption coefficient $\mu(E)$ for silicon.

Finally, Section 5 suggests some directions for future theoretical work.

2. The parameters W and F: previous results

Table 1 summarises some broad-band "material constant" estimates of W and F appearing in the silicon X-ray detector literature from 1969 to date. A comprehensive account of earlier (pre-1968) determinations of these parameters, both experimental and theoretical, is given in

Table 1
Some published values of the "material constants" W and F for X-rays in silicon. Starred entries: papers in which the value of W is cited from the pre-existing literature

Ref.	W (eV)	F	Energy range (keV)	Detector type	Operating temperature (K)
[1]	3.76 *	0.127	1.3 – 4	Si(Li) detector	77
[2]	3.81 *	0.072	0.9 – 5	Si(Li) detector	77
[4]	3.63 ± 0.04 *	–	0.4 – 2	photodiode	300
[5]	3.6 *	–	0.05– 0.25	XUV photodiode	300
[6]	3.63 ± 0.21	–	0.05– 0.25	XUV photodiode	300
[8]	3.68 *	0.11	0.5 – 8	CCD	170
[11]	3.81 *	0.11 ± 0.04	0.18– 1.5	Si(Li) detector	77
[16]	not stated	0.154	14.4 –122	Si(Li) detector	77
[19]	3.70 ± 0.07 *	–	0.5 – 4	photodiode	300
[24]	3.6 *	–	1.5 – 17.5	photodiode	300
[25]	3.81 *	0.132	0.28– 6	Si(Li) detector	77
[26]	3.81 *	0.084 ± 0.005	59.6	Surface barrier	90
[27]	3.65 *	0.16–0.17	1.5 – 5.9	CCD	not stated
[28]	3.8 *	0.098	1.5 – 10	Si(Li) detector	77

Ref. [23]. Since W and F cannot be determined independently from X-ray energy resolution data alone (see Eq. (1)), it is universal practice to assume a value for the former parameter in order to derive a value for the Fano factor. The variation in W exhibited in Table 1 then results, in part, from the distinct operating temperatures of the three main classes of silicon detector and the definitive $W(T)$ measurements of Pehl et al. [29] using 115–1058 keV electrons and 122 keV gamma rays (see Section 3.2). The "value" of F remains uncertain, even at fixed temperature.

Ref. [29] also shows that the ionisation energy at a given temperature depends somewhat on the type of stimulating radiation, with W for alpha particles being less than W for electrons or gamma rays. Yamaya et al. [30] note that there are fundamental differences in the way energy is transferred to the Si electron population where incident photons and protons/alpha particles are concerned. A recent study of light ion interactions in Si [31] has further confirmed a small energy non-linearity in the energy range 35–440 keV. Despite these complications, W and F values appropriate to fast charged particle energy loss in silicon [32,33] are still commonly cited in the X-ray CCD literature.

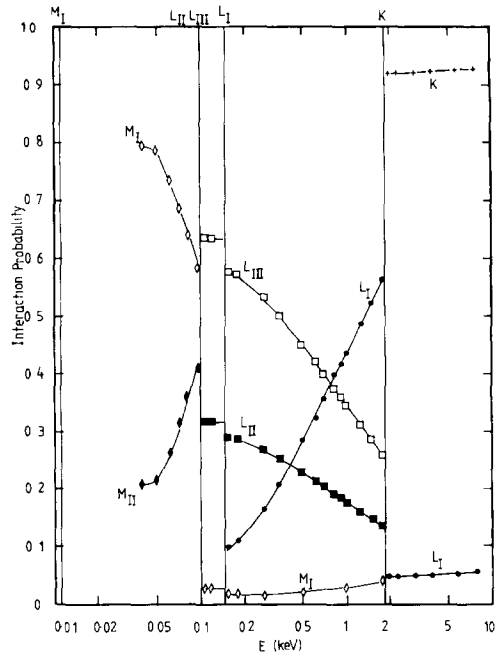

Fig. 1. Probabilities of photoelectric absorption in silicon versus X-ray energy E. Named absorption edges indicated by vertical lines.

3. Monte Carlo calculations

3.1. Physical model

Calculations were carried out for thirty X-ray energies in the range 0.05–8 keV. The number of photon absorptions simulated, N_x, was at least 3×10^4 for all energies; for the twenty-two energies below the silicon K edge, N_x was equal to 10^5. The maximum number of electron histories was 1.74×10^8, for the program run at 8 keV.

3.1.1. X-ray absorption

For each value of E, the relative probabilities of photoelectric absorption by the various silicon electron shells were first determined from the Cromer and Liberman [34] database of *atomic* cross-sections. Fig. 1 shows the dominant interactions in each inter-edge energy region. Above the K edge at 1839 eV, there is a steady $\sim 92\%$ probability of absorption by the K shell electrons. In the region between the L_I and K edges, however, the absorption probability is distributed in an energy-dependent manner between the L_I shell (148.7 eV), the L_{II}/I_{III} shells (assumed degenerate at 99.2 eV) and the M_I (11.4 eV) shell.

3.1.2. Atomic relaxation

For each photon, the comparison of a uniform random number R in the interval [0,1] with a pre-determined absorption probability table determined the type of initial vacancy. Figs. 2a–2c describe the possible relaxation pathways for K-, L_I- and $L_{II,III}$ vacancies, respectively [35,36]. Our Monte Carlo code ignores the (small) probability of L-shell fluorescence and does not allow for the possible reabsorption of K-shell fluorescence photons in the detector volume. The atomic relaxation process is followed until all vacancies, except those due to shakeoff emission, are transferred to the outermost M shell. Shakeoff arises from the abrupt change in atomic central potential which accompanies photoionisation and Auger electron emission. The probabilities of electron shakeoff (from any outer shell) after the creation of a K, L or M_I shell vacancy in silicon were approximated by averaging probabilities for the rare gases Ne and Ar [37]; these averages are listed in Table 2.

The result of the relaxation calculation, for each simulated photon, is a number N_p of primary or "cascade" [20,21] electrons and their associated initial energies. Table 3 shows the primary electron number distributions $P(N_p)$ calculated for X-ray energies $E = 50$, 277, 1800, 2000 and 8000 eV. We note that the probability distributions calculated for the two highest energies are very similar. If the final charge state of the photoionised silicon atom is, as in Xe [13,20], a factor in determining the magnitude of W, we have in Table 3 a first indication that the pair creation energy must be very slowly varying above the Si K edge.

3.1.3. Electron energy loss

In the third and final part of the Monte Carlo calculation, all primary electrons and all the secondaries which they engender are individually followed until their energy E_e falls below a threshold for further ionisation. E_{th}. All

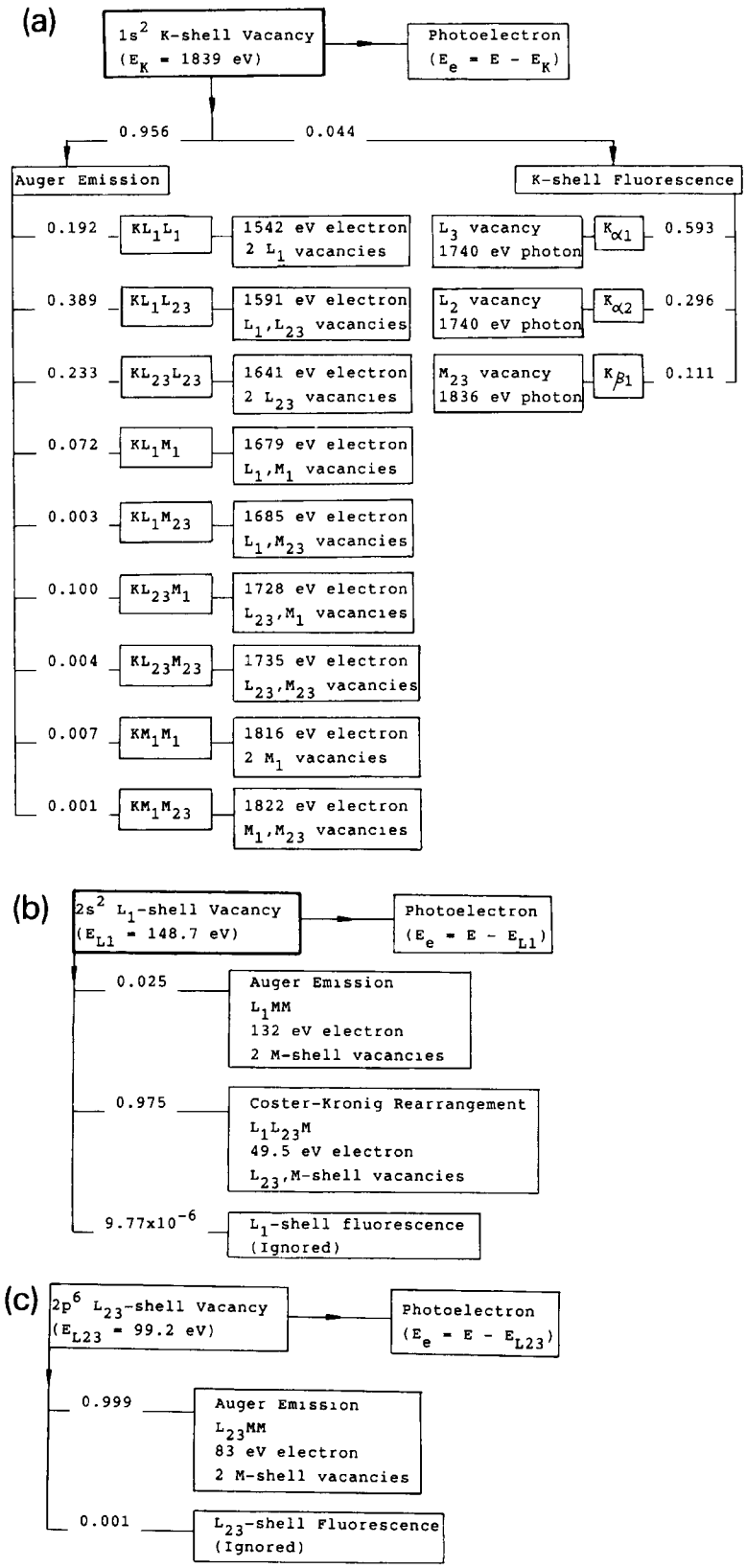

Fig. 2. (a) Probability tree for relaxation of a K-shell vacancy in silicon. The preferred relaxation process is radiationless (95.6% probable) via one of nine Auger electron groups KXY. (b) Probability tree for relaxation of an L_I-shell vacancy. (c) Probability tree for relaxation of an $L_{II,III}$-shell vacancy.

Table 2
Total shakeoff probability $P_s(x)$ and average shakeoff electron energy $E_s(x)$ following sudden creation of a vacancy in silicon shell x

Shell x	$P_s(x)$ (%)	$E_s(x)$ (eV)
K	19.75	19.2
L_I	9.45	6.25
$L_{II,III}$	9.65	6.55
M_I	4.4	2.2

electron energies quoted here are measured relative to the top of the valence band. Five energy loss mechanisms are modelled [38]:

(i) electron–phonon interaction;
(ii) valence band ionisation;
(iii) excitation of plasmons (collective electron oscillations);
(iv) core L-shell ionisation; and
(v) core K-shell ionisation.

For an electron of energy E_e, the probability of the ith process occurring is equal to the inverse mean free path (IMFP) for that process, $\Sigma_i(E_e)$, divided by the total IMFP at that energy.

Note that elastic scattering is assumed to be lossless even in the laboratory frame (in fact, the ratio of the electron mass to the atomic mass is 1.95×10^{-5}) and is ignored. Secondly, the development of the secondary electron charge cloud is assumed to take place in an exactly field-free region so that there is no increase in electron energy between collisions. For ~ keV electrons, the mean free path in silicon is very much less than the depletion depth (~ 10 μm) of even a standard resisitivity CCD, so that this approximation is rather a good one. Finally, we assume that all electrons present when the secondary electron charge cloud is fully developed (i.e. when ionisation ceases) are collected: this energy-loss model contains no device-specific details of imperfect electron transport to an output node.

Table 3
Primary electron number distributions $P(N_p, E)$

N_p	E (eV)				
	50	277	1800	2000	8000
1	0.963	0.009	0.018	0.004	0.004
2	0.037	0.699	0.329	0.037	0.033
3	–	0.242	0.503	0.109	0.106
4	–	0.046	0.136	0.209	0.210
5	–	0.004	0.014	0.282	0.290
6	–	–	0.001	0.224	0.223
7	–	–	–	0.101	0.101
8	–	–	–	0.028	0.027
9	–	–	–	0.005	0.005
10	–	–	–	0.001	–

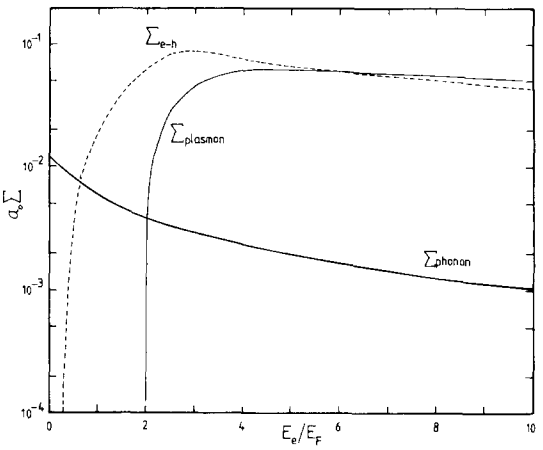

Fig. 3. Normalised inverse mean free path (IMFP) versus normalised electron energy for electron–phonon and electron–plasmon interactions, and for valence band electron–hole pair creation [38]. a_0 is the radius of the first Bohr orbit, 0.53 Å. E_F is the Fermi energy, 12.78 eV [38].

Fig. 3 shows the variation of inverse mean free path with electron energy near E_{th} for electron energy loss processes (i)–(iii) above. The curves are taken from Emerson et al. [38]. The total inelastic IMFPs of Ding and Shimuzu [39] and Tung et al. [40] are in agreement with that of Ref. [38] to within a factor ~ 2. Note that the *effective* ionisation threshold implied by the curve $\Sigma_{e-h}(E_e)$ has the value $E_{th} = 0.2E_F = 2.56$ eV, compared to the $3E_g/2 \sim 1.73$ eV typically used in previous analyses (see, for example, Ref. [33]) E_g denotes the band gap energy for silicon (Section 3.1.3.2) and E_F is the Fermi energy. Note also that plasmon excitation (of the M-shell electrons [32]) is the most probable energy loss mechanism for $E_e/E_F > 6$. Most early calculations of W and F in semiconductors [41,42] took no account of plasmon excitation and were therefore unphysical.

3.1.3.1. Electron–phonon interaction. The electron–phonon IMFP given by Emerson et al. [38] has the simple analytical form:

$$a_0\Sigma = 0.0117(1 + E_e)^{-1} \quad (2)$$

determined by fitting to low-energy ($E_e < 6$ eV or $E_e/E_F < 0.47$) data. It follows, therefore, that the phonon IMFP used in our calculations is an extrapolation for almost all relevant energies. We have, nevertheless, interpreted Eq. (2) as the total IMFP for both electron energy loss and gain during phonon scattering. Following Drummond and Moll [41], we then assumed that the probabilities of phonon emission and absorption (P_{pe} and P_{pa}, respectively) are linked by the temperature-dependent expression:

$$P_{pe}/P_{pa} = \exp(\hbar\omega/kT), \quad (3)$$

where $\hbar\omega$ is the characteristic (optical) phonon energy, 0.052 eV [38,42]. Thus, at the baseline CCD temperature $T = 170$ K employed for most of our calculations, electron energy *loss* by phonon emission is 97.2% probable.

3.1.3.2. Valence band ionisation. We have simplified the partition of energy in valence ionisation by assuming that the energy of the resulting vacancy in silicon, an indirect-gap semiconductor [43] in which conservation of momentum does not guarantee equipartition of energy between electron and hole, is negligible. No other Monte Carlo model is in fact possible, since scattering cross-sections for hole transport are not readily available. For the incident electron in our model:

$$E_e \rightarrow E_e - E_{loss} \tag{4a}$$

while for the new carrier:

$$E_e = E_{loss} - E_g. \tag{4b}$$

The randomised quantity E_{loss} is obtained from a piecewise fit to the differential IMFP $d\Sigma/d\Delta E$ for electron–hole pair creation given by Emerson et al. [38] and by use of the relationship [39]:

$$R = \int_0^{E_{loss}} (d\Sigma/d\Delta E)\, d\Delta E \Big/ \int_0^{E_e} (d\Sigma/d\Delta E)\, d\Delta E. \tag{5}$$

R is, once again, a uniform random number between zero and one.

In common with many previous studies [23,29,41,42], we have used the data of Smith [44] to represent the variation of band gap E_g with temperature. For our baseline temperature $T = 170$ K, $E_g = 1.15$ eV.

3.1.3.3. Plasmon excitation. The average energy loss involved in plasmon excitation by a fast electron is given in Fig. 5 of Emerson et al. [38]. It is equal to $2E_F$ at the plasmon excitation threshold (see Fig. 3 of the present paper) and falls asymptotically to the characteristic plasmon energy $(\hbar\omega)_{pl} = 1.30E_F = 16.6$ eV [32,43] as E_e tends to infinity.

Energy loss to plasmon creation by an "incident" electron of energy E_e can then be characterised by an equation of the form of Eq. (4a), while the energy of all the n electrons (and n holes) resulting from the subsequent decay of the plasmon may be approximated by:

$$E_e = \{(\hbar\omega)_{pl} - nE_g\}/2n. \tag{6}$$

Rothwarf's analysis of plasmon decay [43] suggests that the mean number of electron–hole pairs created by plasmon decay in silicon is 4.6. We have, accordingly, set n equal to 5 in our calculations (see, however, Section 3.2). With this value of n, an ionisation threshold $E_{th} = 0.2E_F$ and $E_g = 1.15$ eV (above), all the resulting charge carriers are indeed non-cascading i.e. incapable of generating still further electron–hole pairs.

3.1.3.4. Core-shell ionisation. The IMFPs for both L- and K-shell ionisation were obtained from the formulae of Emerson et al. [38]:

$$\Sigma = 4\pi a_0^2 N_i \{R_y/E_i\}^2 Q(E_e/E_i), \tag{7}$$

where N_i is the number of electrons per unit volume for the shell in question (1×10^{29} m^{-3} for the Si K shell; 4×10^{29} m^{-3} for the L shell) and $R_y = 13.6$ eV is the Rydberg energy. Q is a dimensionless function of the normalised electron energy (see Fig. 8 of Ref. [38]). E_i represents the characteristic core electron energy, with the obvious attribution of 1839 eV for the K shell. For the L shell we have set E_i equal to the energy of the L_{II}/L_{III} shells, 99.2 eV; in the calculations of W and F presented below, the L_I shell is therefore incompletely represented – present in terms of X-ray absorption, absent in terms of subsequent electron energy loss.

Numerical evaluation of Eq. (7) reveals a maximum value of L-shell IMFP $a_0\Sigma \sim 4.7 \times 10^{-3}$ for $E_e/E_i \sim 4$ ($E_e/E_F \sim 31$). In fact, the total electron IMFP (but not, of course, the energy loss per unit distance or stopping power S) is dominated at all energies by plasmon interactions.

The average energy loss in core shell ionisation has been evaluated from the relationship:

$$E_{loss} = S/\Sigma \tag{8}$$

using the dimensionless functions $S(E_e/E_i)$ and $Q(E_e/E_i)$ plotted by Emerson et al. [38]. The energy loss for the "incident" electron is again described by Eq. (4a), while the energy of the new carrier is obviously:

$$E_e = E_{loss} - E_i. \tag{9}$$

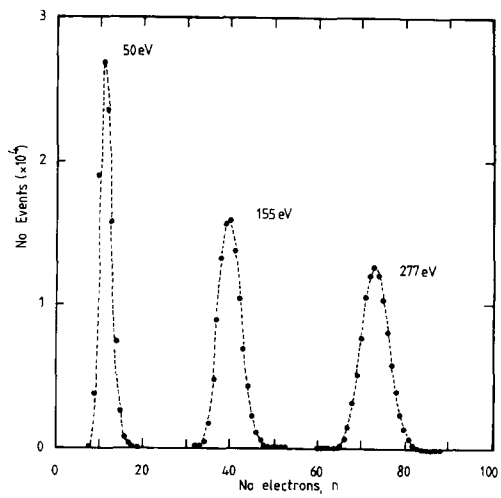

Fig. 4. Electron number distributions for soft X-ray energies. Number of photons simulated: 10^5. Band gap $E_g = 1.15$ eV (operating temperature $T = 170$ K). Coefficient of skewness $\gamma_1 = 0.511$, 0.314 and 0.203 for $E = 50$, 155 and 277 eV, respectively.

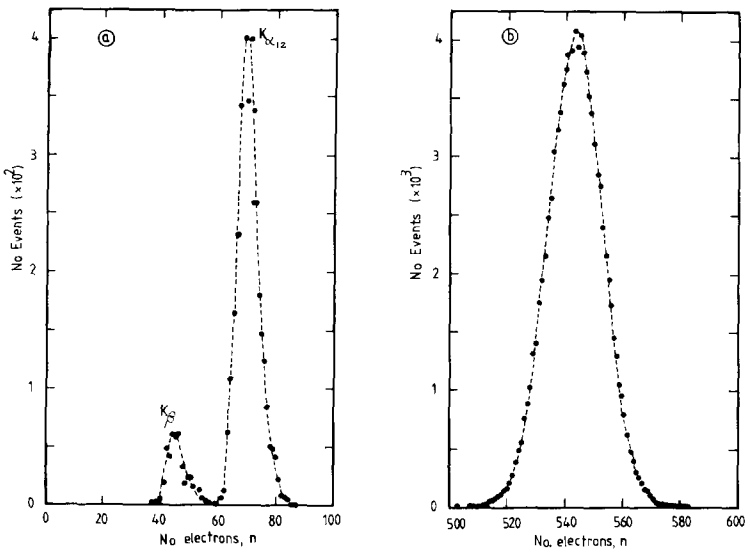

Fig. 5. Electron number distributions resulting from the simulation of 10^5 2000 eV X-rays. Band gap $E_g = 1.15$ eV (operating temperature $T = 170$ K). (a) K-shell escape peaks. (b) Main peak. Note the different vertical scales. The ratio of peak channels in (a) is $45/69 \sim 0.65$, compared to an expected ratio of escape peak energies: (2000–1836) eV/(2000–1740) eV ~ 0.63. The number of events in the K_β escape peak is 476 and in the K_α escape peak, 3688, giving a number ratio of 0.129. The expected value of this ratio can be found from the fluorescence probabilities of Fig. 2a and has the value: $0.111/(0.296 + 0.593) \sim 0.125$.

The creation of each core level vacancy in the simulation is followed by a simplified Auger/shakeoff electron cascade.

3.2. W(E, T) and F(E, T)

For each X-ray energy the parameters W and E were calculated directly from the mean and variance of the output electron number distribution. The computation of F excluded the escape peaks, for $E > 1839$ eV. The calculation of W was found to have converged to within ± 0.001 of its final value after as few as 1000 trials; the larger values of N_x alluded to in Section 3.1 were required in order to ensure convergence of the Fano factor to the same level.

3.2.1. Calculations at constant temperature T = 170 K

Figs. 4 and 5 show typical electron number distributions produced by the model. At low energies ($E < 0.5$ keV), the distributions are markedly asymmetric, with positive, non-zero values of skewness and an excess of events on the high charge side of the peak. It follows, therefore, that the silicon response *cannot* be perfectly represented by a Gaussian distribution at low X-ray energies. This is illustrated in Fig. 6, which shows the integral probability $P(N < n)$ as a function of electron number, n, both for the C K (277 eV) electron number distribution produced by the Monte Carlo model and for two Gaussian

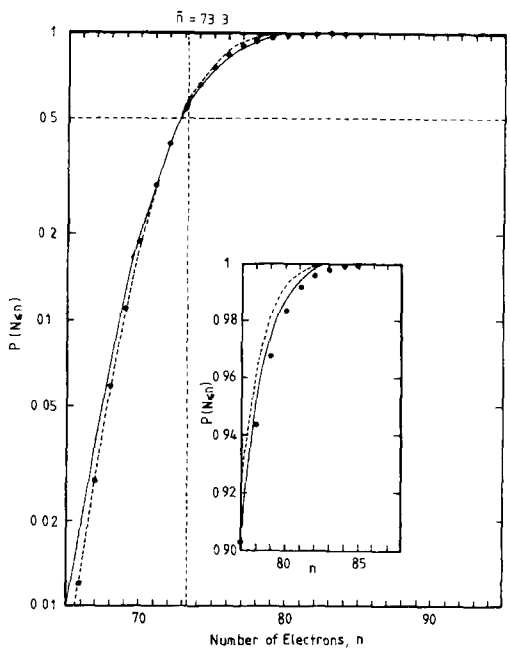

Fig. 6. Gaussian approximation to calculated electron number distribution for C K X-rays ($E = 277$ eV). $E_g = 1.15$ eV (operating temperature $T = 170$ K). Full circles: Monte Carlo electron number distribution; full curve: Gaussian approximation for $\bar{n} = 72.7$ electrons ($W = 3.810$ eV), $F = 0.139$; broken curve: Gaussian approximation for $\bar{n} = 72.7$ electrons and $F = 0.125$. The inset figure shows the range $77 < n < 88$ in more detail.

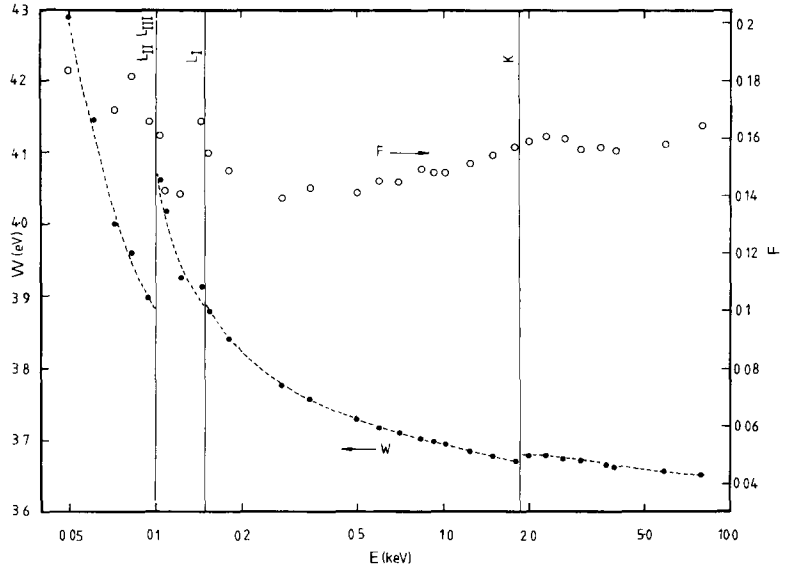

Fig. 7. Variation of the mean electron–hole pair creation energy W (filled circles; left hand scale) and Fano factor F (open circles; right hand scale) with X-ray energy E, $E_g = 1.15$ eV (operating temperature $T = 170$ K). The curve through the $W(E)$ values is drawn to guide the eye.

approximations to it. The mean electron number for the Monte Carlo distribution is $\bar{n} = E/W = 73.3$ electrons (represented by the broken vertical line) which,with the predicted Fano factor of 0.139, implies a standard deviation $\sigma = 3.19$ electrons. The full curve of Fig. 6 is a Gaussian approximation calculated for the same value of σ and a somewhat lower mean electron number, $\bar{n} = 72.7$, determined by the Gaussian symmetry condition $P(N < \bar{n}) = 0.5$. The broken curve of Fig. 6 is the approximation calculated for $\bar{n} = 72.7$ and $\sigma = 3.015$ (an implied Fano factor of 0.125).

Fig. 7 shows the energy-dependence of both W and F for our baseline temperature $T = 170$ K. The mean electron–hole pair energy W exhibits the "sawtooth" variation predicted by Dos Santos et al. [21] for Xe. As in Xe, the variation in $W(E)$ follows the photoionisation cross section. The function $F(E)$, however, is not of the expected form; from the minimum value of 0.140 around 0.5 keV, F *increases* to higher energies. Our estimates of F lie towards the high end of the experimental range summarised in Table 1.

The "step" in gain E/W across the $L_{II,III}$ edges has a magnitude of about 4% or a gap equivalent width [15] of 7 eV. Fig. 8 compares our calculated values of E/W in the vicinity of the L edges with the diode measurements of Kroth et al. [5] and Barbee et al. [6]. Agreement between theory and experiment is good, but the error bars on the measurements are too large to fully validate or invalidate the model. The predicted gain discontinuity across the K edge is much smaller than for the L_{II}/L_{III} edges: approximately 1 electron in 500, or 0.2%. Above the silicon K edge, $W(E)$ tends to an asymptotic value ~ 3.65 eV, in good agreement with experimental values of Table 1. The predicted size of the charge packet resulting from the absorption in silicon of a Mn K_α photon from an ^{55}Fe calibration source, universally used in CCD calibration, is:

$5900/3.658 = 1613$ electrons.

We note that Bichsel [32] cites a private communication from Laegsgaard to the effect that $W(0.56$ keV$)$ exceeds $W(6$ keV$)$ by no more than 1% for soft electrons absorbed in silicon. Our X-ray calculations indicate a similar increase:

$W(0.6\text{ keV})/W(5.9\text{ keV}) = 3.720/3.658 = 1.017.$

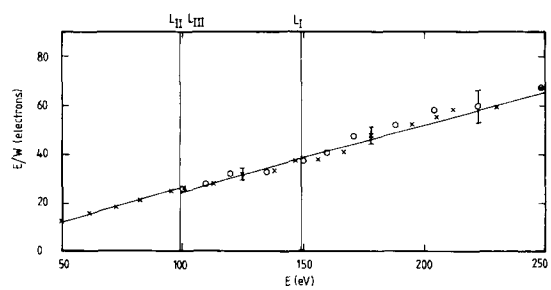

Fig. 8. Variation of gain E/W with X-ray energy E in the vicinity of the silicon L edges (indicated by the vertical lines). Full curve: Monte Carlo model; crosses: photodiode data from Ref. [5]; Circles: photodiode data from Ref. [6]. Typical error bars shown. The experimental points are in fact lower limits, uncorrected for X-ray absorption in the silicon dead layer (only 77 Å thick in the case of Ref [5]).

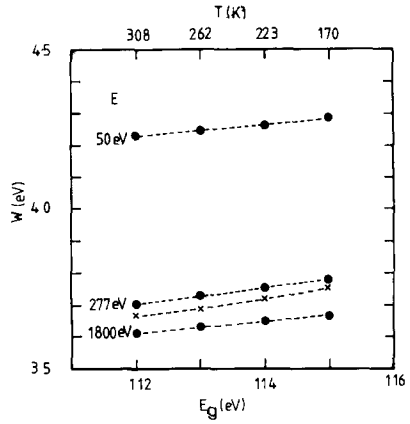

Fig. 9. Variation of W with band gap E_g (bottom scale) or device temperature T (top scale) for three X-ray energies. Crosses: $W(E_g)$ data of Pehl et al. [29] for electrons/γ-rays. For fast electrons, Ryan [46] has reported $W = 3.631$ eV at 300 K and $W = 3.745$ eV at 100 K. Canali et al. [47] have reported a temperature dependence of the form $W = \{2.15E_g(T) + 1.21\}$ eV for alpha particles. Both these data sets are in good agreement with our Monte Carlo prediction for the highest X-ray energy.

Away from the absorption edges, non-constancy of the parameter W implies a non-ideal Si detector response to a continuum input spectrum. The problem is exactly analogous to that of differential non-linearity (DNL) [45] in position sensitive detectors (PSDs). The calibration of a silicon X-ray detector at a series of line energies is analogous to calibration of a PSD through a pinhole mask, which is a measure of integral linearity only. In order to measure local variations in sensitivity (DNL) and so completely characterise the detector response, uniform "flat-field" illumination or its analogue – a continuum input spectrum – is required.

If the number of input photons per unit energy is $A(E)$, the number of counts per output channel x will be:

$$M(x) = \{A(E)Q(E)/K\} \times \{W(E)[1 - (E/W(E))(\mathrm{d}W/\mathrm{d}E)]^{-1}\} \quad (10a)$$

$$= \{A(E)Q(E)/K\}D(E), \quad (10b)$$

where Q is the detector quantum efficiency in counts/photon and K is the system gain in channels per electron. Calculation of the function $D(E)$, based on the results of Fig. 7, reveals, away from the absorption edges, at most a 1% departure from the value 3.679 eV/electron pertaining at 2.15 keV, where $\mathrm{d}W/\mathrm{d}E$ is locally zero. The increasing function E/W and the generally decreasing function $\mathrm{d}W/\mathrm{d}E$ cancel each other rather well.

The Monte Carlo model described in Section 3.1 has essentially no free parameters. Values of W, however, were found to be highly sensitive to the number of electron–hole pairs resulting from plasmon decay (section 3.1.3.3). Trials with $n = 4$ and 6 produced a $\sim 10\%$ increase and decrease in W, respectively, confirming the dominant role of plasmon excitation in the electron energy loss process in silicon (see Fig. 3).

3.2.2. Variation with temperature T

Fig. 9 shows the calculated temperature dependence of the W parameter for three X-ray energies – 50, 277 and 1800 eV. Recall that the temperature T enters the model not only through the band gap function $E_g(T)$ [44] (see Eqs. (4b) and (6)), but also through the ratio of the phonon emission and absorption coefficients (see Eq. (3)). Our calculations are in excellent agreement with experimental determinations of $W(T)$ derived from the literature [29,46,47]. We obtain for the temperature coefficient $\mathrm{d}W/\mathrm{d}T$ an intrinsic value of $\sim 0.01\%\ \mathrm{K}^{-1}$ which is much less than the (on chip amplifier dominated) value of $(0.1 \pm 0.01)\%\ \mathrm{K}^{-1}$ recently measured for a CCD in our laboratory.

The corresponding calculations of $F(T)$ reveal no significant variation of the Fano factor with temperature for either 50 or 1800 eV X-rays and an increase, for C K X-rays, from 0.139 at 170 K to 0.155 at 308 K.

4. Near-edge variation in quantum detection efficiency Q

K-shell Extended X-ray Absorption Fine Structure (EXAFS) is well documented [48] for both amorphous and crystalline silicon; measurements of the linear absorption coefficient $\mu(E)$ in the vicinity of the L edges are also available [49].

Fig. 10 shows the function $\mu(E)$ abstracted from total electron yield measurements obtained for crystalline silicon and X-ray energies in the range 1800–2200 eV on Beamline 3.4 of the Daresbury Synchrotron Radiation

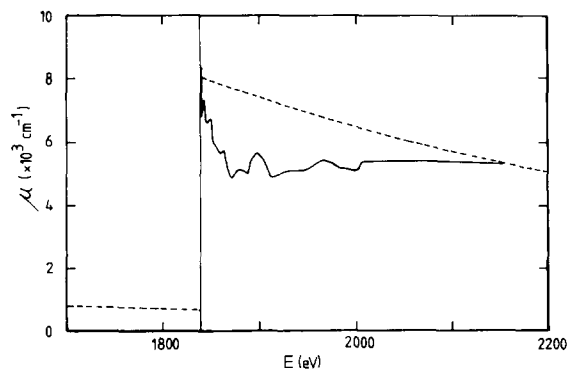

Fig. 10. Near-edge variation of the linear absorption coefficient $\mu(E)$ in silicon. K. absorption edge indicated by the vertical line. Full curve: measurements; broken curve: $\mu(E)$ calculated using atomic database of Cromer and Liberman [34].

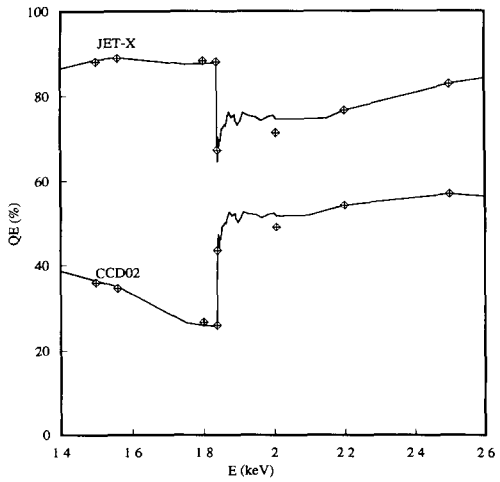

Fig. 11. CCD quantum detection efficiency $Q(E)$ calculated in the vicinity of the silicon K edge. See text for details.

Source (SRS). The photocurrent data was represented by a function of the form:

$$\chi_c = \mu(E)\{a + bE\} \quad (11)$$

and the constants a and b determined by normalisation to values of the linear absorption coefficient calculated at 1800 and 2150 eV using the atomic database of Cromer and Liberman [34].

Fig. 11 shows the results of (1–4 pixel event) quantum detection efficiency calculations for two CCD types:

(i) a standard (type P8603) TV-format device produced by EEV Ltd. (Chelmsford, UK); and

(ii) the large area, deep depletion (type P88930T) CCD produced by EEV for the JET-X project, under contract to the University of Leicester [50].

Both devices consist of three overlapping phases of polysilicon separated from the active detection layer by 0.085 μm thick layers of silicon dioxide and silicon nitride dielectric: a relatively thick layer of oxide (Vapox) covers the device gate structure for passivation and protection (see Fig. 1 of Ref. [50]). The TV-format device (CCD02) is constructed on low resistivity silicon, giving an active depth of 4 μm. The three gates are equal in width and are typically 0.4 μm thick with a 1–2 μm overlap. The Vapox thickness is 0.5 μm. The JET-X device [50], by contrast, is designed for maximum efficiency at both low ($E < 0.5$ keV) and high ($E > 6$ keV) X-ray energies. It is constructed on high resistivity (1500 Ω cm) epitaxial silicon, giving a 37 μm deep active layer. To reduce absorption in the polysilicon gate structure, one electrode is broadened to occupy 63% of the total pixel area and thinned to only 0.17 μm. Finally, the protective oxide layer covering this gate is removed. Oxide coverage is retained above the remaining two phases and overlap regions in order to provide inter-phase isolation.

The diamonds in Fig. 11 represent quantum efficiencies calculated, at a series of isolated energies, on the basis of linear absorption coefficients derived from the Cromer and Liberman database [34]. The quantum efficiency is taken simply to be the product of composite electrode transmission (weighted for fractional pixel coverage of the various structures) and depletion layer absorption. The full curves represent the variation of $Q(E)$ when the silicon mass absorption component of all absorbing materials is derived from the EXAFS curve of Fig. 10. This is only a first approximation to the K-edge structure of real CCDs since, by the very nature of the EXAFS process, the absorption due to Si must depend on its chemical environment – the silicon in, for example, the silicon nitride layer of the chip having a subtly different response from that in the depletion layer. The $Q(E)$ predictions incorporating EXAFS data lie above the "standard" model predictions in the 1.840–2.2 keV range for both CCD geometries; that is, the dominant perturbation to the standard model is the reduced near-edge absorption of the electrode structure in both cases. In the case of the JET-X CCD, there is oscillatory variation in $Q(E)$ above the K edge at the level of several percent.

5. Discussion

We have shown theoretically that departures from ideal linearity in silicon-based X-ray detectors are likely to be small – at or below the 1% level now being demanded as a calibration standard for CCD (and other) detectors in X-ray astronomy. Device non-linearity appears to be less of a practical concern than near-edge variation in detector quantum efficiency. Our calculations of EXAFS contributions to $Q(E)$ in the vicinity of the Si K edge indicate local oscillations with amplitude much higher than 1%.

At the level of fundamental device physics, our calculations of the W parameter are in the substantial agreement with measurements from many sources. Our model further indicates that, above 0.5 keV, the X-ray Fano factor F increases slowly with X-ray energy. This unexpected result is, however, borne out by a careful analysis of JET-X CCD pulse height spectra which, together with both synchrotron and laboratory measurements of the gain "step" at the Si K edge and of near-edge relative quantum efficiency and event morphology, constitutes the second part of our study of the X-ray energy response of silicon [51].

Our Monte Carlo model should also be capable of describing the *spatial* distribution of X-ray induced charge in Si when elastic scattering [52] is added to the suite of microscopic cross-sections used in the present analysis. Such an extension is of interest for the study of CCD "pixel polarimeters" for X-ray astronomy and other fields [53]. The ab initio calculation of W and F for other semiconductor detector media – particularly Ge and GaAs, and concentrating on energies above ~ 10 keV – is a

second area of study on which we hope to report in due course.

Acknowledgements

The authors wish to thank: Dr. S.J. Gurman for providing the raw Si K-shell EXAFS data used to produce Fig. 10 and for introducing us to the standard EXAFS analysis equation (Eq. (11)); Dr. C. Castelli (Dept. of Electronics, University of York), whose early measurements of CCD gain change across the Si K edge led to this study being undertaken. Calculations of W, F were made using a University of Leicester Computer Centre SGI Challenge XL computer. The work of the Leicester X-ray Astronomy Group is supported by the UK Particle Physics and Astronomy Research Council.

References

[1] Y. Inagaki, K. Shima and H. Maezawa, Nucl. Instr. and Meth. B 27 (1987) 353.
[2] M. Krumrey, E. Tegeler and G. Ulm, Rev. Sci. Instr. 60 (1989) 2287.
[3] J.L. Campbell, Nucl. Instr. and Meth. B 49 (1990) 115.
[4] M. Krumrey and E. Tegeler, Nucl. Instr. and Meth. A 288 (1990) 114.
[5] U. Kroth, T. Saito and E. Tegeler, Appl. Opt. 29 (1990) 2659.
[6] T. Barbee et al., Opt. Eng. 30 (1991) 1067.
[7] K.W. Wenzel, C.K. Li, R.D. Petrasso, D.H. Lo, M.W. Bautz, G.R. Ricker and E. Hsieh, Rev. Sci. Instr. 64 (1993) 1723.
[8] A. Wells et al., Proc. IAU Colloquium 115 on High Resolution Spectroscopy of Cosmic Plasmas, eds. P. Gorenstein and M.V. Zombeck (Cambridge University Press, (1990) 318.
[9] G.F. Bignami et al., Proc. SPIE 1344 (1990) 144.
[10] K.A. Weaver, Ph.D thesis, Univ. Maryland (1993).
[11] R.G. Musket, Nucl. Instr. and Meth. 117 (1974) 385.
[12] J.C. Lochner and E.A. Boldt, Nucl. Instr. and Meth. A. 242 (1986) 382.
[13] P. Lamb, G. Manzo, S. Re, G Boella, G. Villa, R. Andresen, M.R. Sims and G.F. Clark, Astrophys. Space Sci. 136 (1987) 369.
[14] K. Jahoda and D. McCammon, Nucl. Instr. and Meth. A 272 (1988) 800.
[15] H. Tsunemi, K. Hayashida K. Torii, K. Tamura, E. Miyata, H. Murakami and S. Ueno, Nucl. Instr. and Meth. A. 336 (1993) 301;
See also J.M.F. dos Santos, C.A.N. Conde and A.C.S.S.M. Bento, Nucl. Instr. and Meth. A 324 (1993) 611.
[16] H. Zulliger, L.M. Middleman and D.W. Aitken, IEEE Trans. Nucl. Sci. NS-16 (1969) 47.
[17] A. Bianconi, A. Di Cocco, N.V. Pavel, M. Benfatto, A. Marcelli, C.R. Natoli, P. Pianetta and J. Woicik, Phys. Rev. B 12 (1987) 6426.
[18] T. Cho, N. Yamaguchi, T. Kondoh, M. Hirata, S. Miyoshi, S. Aoki, H. Maezawa and M. Nomura, Rev. Sci. Instr. 59 (1988) 2453.
[19] N. Ahr and E. Tegeler, Nucl. Instr. and Meth. A 319 (1992) 387.
[20] T.H.V.T. Dias, F.P. Santos, A.D. Stauffer and C.A.N. Conde, Nucl. Instr. and Meth. A 307 (1991) 341.
[21] F.P. Santos, T.V.H.T. Dias, A.D. Stauffer and C A.N. Conde, Nucl. Instr. and Meth. A 307 (1991) 347
[22] A. Akkerman, A. Gibrekhterman, A. Breskin and R. Chechik, J. Appl. Phys. 72 (1992) 5429
[23] G. Restelli and A. Rota, in: Semiconductor Detectors, eds. G. Bertolini and A. Coche (North-Holland, Amsterdam, 1968).
[24] K.W. Wenzel, C-K Li, R.D. Petrasso, D.H. Lo, M.W. Bautz, G.R. Ricker and E. Hsieh, Rev. Sci. Instr. 64 (1993) 1723.
[25] J.M. Jaklevic and F.S. Goulding, IEEE Trans. Nucl. Sci. NS-18 (1971) 187.
[26] J.E. Eberhardt, Nucl. Instr. and Meth. 80 (1970) 291.
[27] J. Janesick, T. Elliott, R. Bredthauer, C. Chandler and B. Burke, Proc. SPIE 982 (1988) 70.
[28] S. Goto, Nucl. Instr. and Meth. A 333 (1993) 452
[29] R.H. Pehl, F.S. Goulding, D.A. Landis and M. Lenzlinger, Nucl. Instr. and Meth. 59 (1968) 45.
[30] T. Yamaya, R. Asano, H. Endo and K. Umeda, Nucl. Instr. and Meth. 159 (1979) 181.
[31] P. Bauer and G. Bortels, Nucl. Instr. and Meth. A 299 (1990) 205.
[32] H. Bichsel, Rev. Mod. Phys. 60 (1988) 663.
[33] R.C. Alig, S. Bloom and C.W. Struck, Phys. Rev. B 22 (1980) 5565.
[34] D.T. Cromer and D. Liberman, LASL report LA-4403 (1970).
[35] V.O Koustroun, M.H. Chen and B. Crasemann, Phys. Rev. A 3 (1971) 533.
[36] W.Bambynek, B. Crasemann, R.W. Fink, H.U. Freund, H. Mark, C.D. Swift, R.E. Price and P. Venugopala Rao, Rev. Mod. Phys. 44 (1972) 716.
[37] T.A. Carlson and C.W. Nestor, Phys. Rev. A 8 (1973) 2887
[38] L.C. Emerson, R.D. Birkhof, V.E. Anderson and R.H. Ritchie, Phys. Rev. B 7 (1973) 1798.
[39] Z-J. Ding and R. Shimuzu, Surf. Sci. 197 (1988) 539.
[40] C.J. Tung, J.C. Ashley and R. H. Ritchie, Surf. Sci. 81 (1979) 427.
[41] W.E. Drummond and J.L. Moll, J. Appl. Phys. 42 (1971) 5566.
[42] H.R. Zulliger, J. Appl. Phys. 42 (1971) 5570.
[43] A. Rothwarf, J. Appl. Phys. 44 (1973) 752.
[44] R.A. Smith, Semiconductors (Cambridge University Press, 1959).
[45] M.A. Barstow, G.W. Fraser and S.R. Milward, Proc. SPIE 597 (1985) 352.
[46] R.D. Ryan, IEEE Trans. Nucl. Sci. NS-20 (1973) 478.
[47] C. Canali, M. Martini, G. Ottaviani and A. Alberigi Quaranta, IEEE Trans. Nucl. Sci, NS-19 (1972) 9.
[48] A. Bianconi, A. Di Cocco, N.V. Pavel, M. Benfatto, A. Marcelli, C.R. Natoli, P. Pianetta and J. Woicik, Phys. Rev. B 12 (1987) 6426.
[49] C. Gahwiller and F.C. Brown, Phys. Rev. B 2 (1970) 1918.
[50] K.J. McCarthy and A. Wells, Proc. SPIE 1743 (1992) 211.
[51] A. Owens, A.F. Abbey, A. Holland, K. McCarthy, A. Keay, A. Smith, V. Suller, G.W. Fraser and A. Wells, The X-ray energy response of silicon: (B) Measurements to be submitted to Nucl. Instr. and Meth. A.
[52] S. Ichimura and R. Shimuzu, Surf. Sci. 112 (1981) 386.
[53] H. Tsunemi, K. Hayashida, K. Tamura, S. Nomoto, M. Wada, A. Hirano and E. Miyata, Nucl. Instr. and Meth A 321 (1992) 629.